2017-07

# Creep analysis of concrete containing rice husk ash

He, Z-H



10.1016/j.cemconcomp.2017.03.014
Cement and Concrete Composites
Elsevier BV

Submitted 23 October 2015 (Cement and concrete Composites)
Accepted 15 March 2017
Published 26 March 2017 (http://dx.doi.org/10.1016/j.cemconcomp.2017.03.014)

# Creep analysis of concrete containing rice husk ash

Zhi-hai He[1, 2], Long-yuan Li[2], Shi-gui Du[1]

1) College of Civil Engineering, Shaoxing University, Shaoxing 312000, China

2) School of Marine Science and Engineering, University of Plymouth, PL4 8AA, UK

**Abstract** – This paper presents an experimental study on the mechanical properties of concrete added with rice husk ash (RHA) as a supplementary cementitious material. The compressive strength, modulus of elasticity and creep were obtained experimentally from specimens with different RHA contents (0%, 10%, 15% and 20% of binder). The results show that the addition of RHA in concrete can improve both the compressive strength and modulus of elasticity and reduce the creep of concrete. The examination of pore micro-structure of hardened concrete using both the mercury intrusion porosimetry and scanning electron microscope techniques demonstrates that RHA particles can react with calcium hydroxide originated from cement hydration to produce additional C-S-H, which can fill voids and large pores and thus reduces the porosity related to capillary pores and voids. In addition, the release of absorbed water, which is retained in the small pores of RHA particles at early days, can improve cement hydration and thus reduce the porosity related to gel pores.

**Keywords**: Concrete, rice husk ash, compressive strength, elastic modulus, creep.

## 1. Introduction

Rice husks are the coatings of seeds, or grains, of rice. They are formed from hard materials, including opaline silica and lignin, to protect the seed during the growing season. Rice milling industry generates substantial rice husk during milling of paddy, which is mostly used as fuels in boilers for processing of paddy and in power stations for electricity generation. Rice husk ash (RHA) is about 25% by weight of rice husk when burnt in boilers.

RHA is a carbon neutral green product which contains more than 60% silica ($SiO_2$), 10–40% carbon and other minor mineral composition. Because of its availability and almost free of cost, the exploration of the use of RHA becomes interesting and has been a hot research topic in recent years [1,2]. For example, Witoon [3], Zeng and Bai [4] described the use of RHA to produce porous silicas of different meso-pore diameters for $CO_2$ capture. Azadi et al. [5] utilized RHA as filler for epoxy paint and investigated the influence of RHA on the mechanical properties of cured coatings. Tipsotnaiyana et al. [6] described the synthesizing process of silica powder from RHA for printing raw materials application. Bondioli et al. [7] reported the screening results of the scientific activity conducted on the possibility of using RHA as silica precursor for ceramic

pigments. Andreola et al. [8] reported the results of an evaluation of the use of RHA as the source of silica in the preparation of coral ceramic pigments. Owing to its low thermal conductivity [9], RHA has also been used as a thermal insulator in fire protected bricks [10]. In addition, attempts have been made to use RHA as filler for natural and synthetic rubbers [11,12] and to produce high purity polycrystalline silicon for semiconductor devices in computer industry [13,14].

Apart from the applications described above, a big use of RHA is probably in the fields of composite and concrete materials. Because of its high silicon content, RHA can be treated as a raw material for the production of a series of silicon-based materials including $SiO_2$, SiC, $Si_3N_4$, $Mg_2Si$ and carbon enriched materials which can be used in metal matrix and ceramic matrix composites [15-19]. The use of pozzolan as alternatives for ordinary Portland cement has been practiced for several decades in order to reduce $CO_2$ emissions and the production cost of concrete, as well as improve the performance and durability of produced concrete. In recent years, RHA has been increasingly used as a supplementary cementitious material (SCM) to partially replace ordinary Portland cement in concrete [20-23]. It is reported that as many as 30% of Portland cement can be replaced with RHA [24-26]. Bakar et al. [27] examined the influence of RHA fineness on the physical and chemical properties of concrete. It was found that, when a RHA dosage of 15% by weight of binder was used the RHA ground for the optimum grinding time had a median particle size of 9.52 μm. The effectiveness of unground low-carbon RHA as a pozzolan and the effect of grinding the RHA to finer

fractions for use in Portland cement systems were investigated by Venkatanarayanan et al. [28]. The properties investigated include the setting time and calcium hydroxide depletion of RHA pastes, microstructure and flow behaviour of RHA mortars, strength and durability of RHA concretes. Results from this investigation suggested that the unground RHA and ground RHA mixtures performed better than the traditional concrete mixtures without RHA in all tests conducted except water demand and setting time. Bui et al. [29] investigated the effect of particle sizes involved in RHA-blended Portland cement on the compressive strength of concrete by using a combined mechanical and computer simulation, which demonstrated that the favourable results for coarser cement reflect improved particle packing structure accompanied by the decrease in porosity and in particle spacing. Isaia et al. [30] conducted an experimental study on the physical and pozzolanic action of mineral additions on the mechanical strength of high-performance concrete. They tested 12 concrete mixtures, one with Portland cement, nine with 12.5%, 25% and 50% of replacement of cement by fly ash, RHA and limestone filler, two with (12.5+12.5)% and (25+25)% of fly ash and RHA. All mixtures were prepared with water/binder ratios of 0.35, 0.50, and 0.65. The results show that the pozzolanic and physical effects have increased as the mineral addition increased in the mixture and the pozzolanic effect was stronger in the binary and ternary mixtures prepared with RHA in proportions of 25% or higher. Coutinho [31] presented a laboratory study of controlled permeability formwork applied to concrete where cement was partially replaced (10%, 15% and 20%) with RHA. His results showed that the controlled permeability formwork can improve concrete performance

even further when using partial cement replacement by RHA. The effect of RHA on concrete durability has been studied by several researchers [32-36]. Sensale [32] presented an experimental investigation on the effects of partial replacements of Portland cement by RHA on the durability of both conventional and high performance concretes. His results show that addition of RHA in both concretes leads them to have different behaviours in air permeability and chloride penetration, depending on the water/binder ratio used. Chalee et al. [33] reported the effects of ground rice husk–bark ash (GRBA) on the compressive strength, chloride diffusion coefficient, chloride binding capacity, and steel corrosion of concrete exposed to a tidal zone of seawater in the Gulf of Thailand for five years. The results showed that during 5-year exposure, GRBA concretes gained strength faster than Type I Portland cement concretes and no strength loss was found in GRBA concrete. The findings indicated that the durability of concrete in terms of chloride diffusion coefficient, chloride binding capacity, and resistance to corrosion of embedded steel could be improved by the use of GRBA. Jaya et al. [35] investigated the compressive strength and microstructure of concrete containing RHA under seawater attack by wetting and drying cycles. The performance of RHA blended cement concretes subjected to sulphate environment was studied recently by Hossain and Anwar [36]. The use of RHA in self-compact concrete [37,38] and geopolymer concrete [39-41] was also reported in literature.

The aforementioned literature survey shows that, despite the considerable amount of work published in literature on RHA and its effect on concrete properties when it is

used as a SCM, there is very little work on the effect of RHA on the creep and shrinkage of concrete [25,42]. Creep is defined as the deformation of a structure under sustained load. For concrete the creep originates from the C-S-H in the hardened Portland cement paste, which is fundamentally different from the creep of metals and polymers [43]. In general, the creep rate of concrete increases with applied stress. However, there are additional factors that can also influence the concrete creep and shrinkage, which include water content, curing conditions, relative humidity, aggregate proportions, and specimen sizes. Concrete creep has received considerable attention from both academics and practical engineers. Pihlajavaara provided a good review on the early research on the ageing phenomena of concrete including the effect of moisture conditions on strength, shrinkage and creep of mature concrete [44]. Li and Yao reported a study on the creep and drying shrinkage of high performance concrete [45]. Note that the cement type and the use of SCMs can also affect the strain behaviour of the mixed concrete since the SCMs can modify the pore size distribution and the characteristics of the interfaces. This has been demonstrated by the research work conducted on the effect of different SCMs on the mechanical properties of normal concrete [46] and high performance concrete [47], and the creep and shrinkage of concrete with SCMs [48,49]. For example, it was reported that the addition of metakaolin in concrete can reduce the creep of mixed concrete [48]; but the concrete with higher GGBFS percentage exhibits higher creep and shrinkage strains [49].

Creep and shrinkage can cause a major loss of pre-stress in pre-stressed concrete. Underestimation of multi-decade creep can lead excessive deflections in large-span pre-stressed RC beams. Due to creep effects, the long-term deformation of RC structures can be significantly larger than their corresponding short-term deformation. Creep may cause excessive stress and cracking in cable-stayed or arch bridges, and roof shells. Non-uniformity of creep and shrinkage, caused by differences in the histories of pore humidity and temperature, age and concrete type in various parts of a structure may lead to cracking. The creep effects are particularly important for pre-stressed concrete structures because of their slenderness and high flexibility. At high temperature exposure, such as in fire or postulated nuclear reactor accidents, creep is very large and plays a major role in the degradation of structural performance. In this paper, a study on the analysis of creep in concrete mixed with RHA as a SCM is presented. The effect of RHA on the creep of mixed concrete is examined using an experimental method. To support the findings obtained from the creep experiments, pore-structure analysis for concretes with different levels of RHA is also carried out using mercury intrusion porosimetry (MIP) and scanning electron microscope (SEM) techniques.

## 2. Experimental

When a concrete material is loaded, it undergoes elastic and inelastic deformations. Elastic deformations occur immediately after the concrete is subjected to a given load,

according to Hooke's Law. Inelastic deformations increase with time as the concrete experiences a sustained load. This inelastic deformation is known as creep and it increases at a decreasing rate during the loading period. The amount of creep that the concrete undergoes is dependent upon several factors, including the magnitude of the sustained loading, the age and strength of the concrete when the stress is applied, and the total amount of time that the concrete is stressed. Note that when the concrete is loaded, the specimen may undergo internal changes such as closure of voids in the concrete, viscous flow of the cement-water paste, crystalline flow in aggregate, and water flowing out of the cement pores due to drying and loading. Aggregates play an important role in both creep and shrinkage. A well graded, coarser aggregate with low voids content decreases the effects of creep and shrinkage. Also, hard, dense aggregates that are not absorptive and have a high modulus of elasticity are desirable for low shrinkage and creep rates [43]. Another important aspect to reducing creep is the type of curing procedure performed prior to loading. Atmospheric and high-pressure steam curing produces little creep when compared to the seven-day moist curing method. Other factors affecting creep include type of cement, amount of cement paste, size and shape of concrete, amount of reinforcement, volume-to-surface ratio, temperature, and humidity. This indicates that the analysis of concrete creep is a difficult task and any creep experiments to be carried out need be carefully designed in order to obtain meaningful data.

## 2.1 Materials

The cement used in the experiments was normal ordinary Portland cement (PC). The RHA used was supplied by a local company which was produced by a controlled burning of rice rusk under guided and enclosed place. Table 1 shows the chemical properties of the PC and RHA used in the experiments, which shows that the RHA has far more $SiO_2$ but much less CaO than the PC does.

The particle size distributions of PC and RHA were determined by laser particle analysis using BT-9300 Laser Particle Analyzer, which are shown in Fig.1. It can be seen from the figure that the size range of RHA particles is wider than that of PC particles. However, in terms of the average size, RHA particle is smaller than PC particle.

The specific gravities of PC and RHA are about 2940 and 2110 kg/m$^3$, respectively, which were determined according to British Standard (BS 1377: Part 2) using the small pycnometer method. The specific surface area is about 370 m$^2$/kg for PC and 62000 m$^2$/kg for RHA, respectively, which were determined based on the nitrogen adsorption method. Note that, unlike cement, RHA is a porous material. This is why its specific surface area is much greater than that of PC. In addition, RHA particles are irregular in shape, which can be demonstrated in the SEM image shown in Fig.2.

River sand was used for fine aggregates, which has a fineness modulus of 2.3 and a

specific gravity of 2480 kg/m$^3$. Crushed granite was used for coarse aggregates, which has a size range from 5.0 mm to 25 mm, and a specific gravity of 2630 kg/m$^3$. The specific gravity as well as the absorption tests for both fine and coarse aggregates were done as specified in ASTM C127‑88 and ASTM C128-97, respectively. The sieve analysis was done in compliance with BS 882:1992.

## 2.2 The concrete mixture proportioning

Mixture proportioning was carried out according to Chinese standard for concrete mix design method. The targeted compressive strength was 50 MPa for the PC control mixture. In order to maintain the high workability of the concrete mixtures, a polycarboxylate ether-based superplasticizer with a specific gravity of 1200 kg/m$^3$ was used, which allows a water reduction up to 25%.

Four types of concrete mixtures of different RHA contents (0%, 10%, 15% and 20% of binder) were used in the experiments. In all types of mixtures the binder to aggregate ratio, fine to coarse aggregate ratio, and water to binder ratio were kept as constants, which are 0.26, 0.40, and 0.40, respectively. The superplasticizer content was adjusted to maintain a slump of 140-160 mm for all mixtures. Table 2 shows the details of the components used in the mixtures.

## 2.3 Test methods

Three groups of specimens were casted for each mixture. One is for the compressive strength test, in which the dimensions of the specimens are 150 mm x 150 mm x 150 mm. One is for the elastic modulus test, in which the dimensions of the specimens are 150 mm x 150 mm x 300 mm. One is for the creep test, in which the dimensions of the specimens are 100 mm x 100 mm x 300 mm.

For the compressive strength and elastic modulus tests, after mixing and casting, the specimens were kept in moulds for about 24 hours at room temperature (20±5) $^{o}$C. After that, they were demoulded and placed in a standard curing room of controlled temperature (20±2) $^{o}$C and relative humidity more than 95% for 27 day curing before they were tested (that is a total of 28 days from mixing to testing). Both the compressive strength and elastic modulus tests were carried out using Instron testing machine, by following the standard for test method of mechanical properties on ordinary concrete (Chinese GB/T 50081-2002).

For the creep test, when they were casted all specimens had a digital humidity sensor and a vibration string type strain gauge (about 130 mm in length) embedded at the middle of the specimens (see Fig.3a) along their axial direction. After mixing and casting, specimens were kept in moulds for about 24 hours at room temperature (20±5) $^{o}$C. After that, they were demoulded and placed in a standard curing room of controlled temperature (20±2) $^{o}$C and relative humidity more than 95% for another 6

days (that is a total of 7 days from mixing to testing) before they were tested in creep testing machine. During the creep tests the temperature and relative humidity were controlled at about (20±2) $^{o}$C and (60±5) %, respectively.

The experimental setup for measuring creep is shown in Fig.3b. It is composed of a frame with four steel bars, together with two thick steel plates. Two prismatic specimens, 100 x 100 mm in side lengths and 300 mm in height, separated by a thin steel plate, were placed between the two thick steel plates. The bottom steel plate was supported by a strong spring of stiffness 4 kN/mm, fixed on the platform of the testing machine (see Fig.3b). A constant load, corresponding to 25% of the cubic compressive strength of the specimen obtained at 28 days, was applied along the axial direction of the specimens by compressing the spring. Four dial indicators placed along the tested specimens were used to indicate the loading direction and to ensure the loading was applied along the axial direction of the specimens. The creep under the constant load was monitored by the axial strain recorded in the embedded strain gauge and the relative humidity recorded in the embedded digital humidity sensor. Note that the strain recorded from the embedded strain gauge involves not only the creep strain but also the drying shrinkage strain. In order to eliminate the drying shrinkage strain, a separate test of the specimen without loading was carried out for each tested specimen, from which the drying shrinkage strain was obtained. The creep strain thus was calculated from the difference between the strains obtained from the creep and drying shrinkage tests. Note that both the creep strain and drying shrinkage

strain obtained from the tests included the autogenous shrinkage. Thus, strictly speaking, they should be treated as the total creep and total shrinkage. However, since both tests were carried out for specimens after the 7 days curing the autogenous shrinkage would be very small and thus it is not considered in the present study. Table 3 summarizes the tests carried out for the three groups of specimens.

MIP and SEM techniques were used to measure the pore size and its distribution and to examine the pore microstructure in hardened concrete specimens containing RHA (normally 180 days). The MIP used is able to generate pressures up to 420 MPa and measure pores of diameters ranging from 3.5 nm to 400 μm. The specimens used for the MIP and SEM tests were first broken into small pieces of size 3-5 mm, which consist of only mortar and fine aggregates, and then stored in ethanol solution for 3 days to prevent further hydration and/or carbonation. After then, they were dried and stored in sealed containers before the MIP and/or SEM tests were carried out.

## 3. Results and discussions

### 3.1 Compressive strength and elastic modulus

Compressive strength was obtained by using pure uniaxial compression. The cubic compressive strength was calculated by using the maximum load divided by the original cross-section area of the specimen. Fig.4 shows the variation of the

compressive strength with the RHA content added in the concrete mixture. Each result presented here is the average value of three tested specimens with identical mixture, and the error bar represents the variation of the obtained data. It is seen from the figure that the compressive strength increases with the increase of RHA content. However the rate of increase becomes slow when the RHA-to-binder ratio reaches to 15%. This finding seems to be consistent to what was reported in literature. For example, Safiuddin et al. [50] reported that a better compressive strength was achieved for the mix containing 15% RHA. Similar result was also reported by Chopra et al. [51], who found that the compressive strength increased with the percentage of RHA up to 15% replacement. However, Kannan et al. [52] found that the compressive strength decreased with the increase in RHA for RHA-to-binder ratio greater than 20%. Gastaldini et al. [53] found that the highest 28 day compressive strength for water-to-binder ratios of 0.35 and 0.50 was the mix with 30% RHA substitution; whereas the optimum compressive strength for a water-to-binder ratio of 0.65 was the mix with 5% RHA substitution. This indicates that the effect of RHA on the compressive strength also depends on water-to-binder ratio, in addition to the percentage of RHA used in the binder.

The modulus of elasticity of the specimen was determined by loading the specimen in its axial direction to 40% of the compressive strength of the specimen used in the cubic strength test, followed by unloading. During the test the stress was calculated by the actual load divided by the original cross-section area of the specimen, whereas the

strain was measured directly by using the clip-on extensometers, which were attached on the central part of the specimen. Fig.5 shows the typical loading and unloading stress-strain curves obtained from a set of specimens. In order to avoid the error caused during the transition from loading to unloading, only the part of the unloading stress-strain curve between the stresses of 2.5 MPa and 10 MPa was used to calculate the secant slope from which the modulus of elasticity was obtained. Fig.6 shows the variation of the elastic modulus with the RHA content added in the concrete mixture. Similarly to the compressive strength, the data shown here is the average value of three tested specimens with identical mixture, and the error bar represents the variation of the obtained data. It can be seen from the figure that the variation of the elastic modulus with the RHA is very similar to that of the compressive strength. Only difference is that, when the RHA-to-binder ratio is greater than 15%, the increase of elastic modulus is slightly higher than the increase of compressive strength.

### 3.2 Creep

During the creep test of a specimen the applied load was controlled by a loading sensor and kept unchanged, whereas the strain and IRH were obtained directly from the strain gauge and digital humidity sensor embedded in the specimen. The creep strain was calculated by using the strain obtained from the creep test subtracting the corresponding drying shrinkage strain obtained in a separate test as described in preceding section. Fig.7 shows the creep strain of the specimens with different

RHA-to-binder ratios at different loading times. Each result is the average value obtained from 2x2 tested specimens with identical mixture, whereas the error bars show the variation of the obtained data. The corresponding drying shrinkage of the specimens is plotted in Fig.8. It appears that for each mixture the creep strain and drying shrinkage strain have similar tendency, although in terms of the value the creep strain is more than twice of the drying shrinkage strain. It can be observed from Fig.7 that, all of the specimens exhibit a similar variation trend, in which the creep increases quickly with the loading time for the first 60 days, but after then the increasing rate becomes very slow and tends to be stable. In general, the specimen with a higher RHA-to-binder ratio has a smaller creep strain, but the influence of RHA on the creep seems unequally. For example, adding 10%, 15% and 20% RHA in binder reduces the creep at 60 days since the loading by 17%, 30%, and 33%, respectively. This indicates that there is an up-limited effect of RHA on the creep. Of the three mixtures 15% RHA seems to be the best in terms of the reduction of the creep. Note that the creeps shown in Fig.7 were obtained from the compressive tests with constant axial stresses. To eliminate the effect of stress scale on the creep, one usually uses the creep coefficient, which is defined as the ratio of the creep strain to the elastic strain as follows,

$$C_{cr} = \frac{\varepsilon_{cr}}{\varepsilon_{el}} = \frac{\varepsilon_{cr}}{\sigma / E} = \frac{4\varepsilon_{cr}}{f_c / E} \quad (1)$$

where $C_{cr}$ is the creep coefficient, $\varepsilon_{cr}$ is the creep strain, $\varepsilon_{el}$ is the elastic strain, $\sigma$ is the applied compressive stress ($\sigma$ = 0.25$f_c$ in the present experiments), $f_c$ is the cubic compressive strength of the specimen, and $E$ is the modulus of elasticity. Note that,

strictly speaking, the modulus of elasticity used in Eq.(1) should be measured at the same time as the creep strain was measured. However, compared to the creep strain, the variation of the modulus of elasticity with concrete age is rather small particularly when the specimen has already been cured for 7 days before it is tested. Therefore, in the present study only the modulus of elasticity at 28 days was used for the calculation. Using Eq.(1), the four curves shown in Fig.7 can be re-plotted as the curves of creep coefficient versus the loading time, which are shown in Fig.9. It can be seen from the figure that the variation of creep coefficient with the loading time is very similar to that of creep with the loading time. This indicates that the effects of RHA on the compressive strength and elastic modulus are very comparable.

Fig.10 shows the variation of the ratio of creep coefficients, $C_{cr}/C_{cro}$, of specimens with and without RHA, where $C_{cro}$ is the creep coefficient of the specimen without RHA. It can be seen from the figure that the overall tendency of the curves for the three mixtures with different RHA levels is very similar although their values are different. Before the loading time reaches to 60 days, the ratio of creep coefficients increases almost linearly with the time; while after 60 days loading, the ratio of creep coefficients tends to be stable. Fig.11 graphically shows the effect of RHA on the ratio of creep coefficients at 180 days since the loading. It is evident from the figure that the more the RHA added in concrete the lower the ratio of creep coefficients, but the relationship between them is not linear. In particular, after RHA is greater than 15% of the binder in weight, the reduction of the creep for further addition of RHA seems to

be limited.

It is known that the creep of concrete is largely induced by the change of internal relative humidity (IRH). Fig.12 shows the evolution of IRH in each tested specimen, which were recorded from the embedded digital humidity sensor. Although the IRH used here reflects the humidity only at the center of the specimen and in reality the IRH would not be uniformly distributed in the cross-section of the specimen, it is evident from the figure that the central IRH in all specimens decreases quickly with the loading time during the first 60 days. After then the decrease becomes very slow. This is well correlated with the change of creep found in the specimens shown in Fig.7. Also, it can be seen from the figure that, the addition of RHA in binder can slow down the reduction of IRH. For example, the IRHs of the specimens with 0%, 10%, 15% and 20% RHA at 180 days since the loading are 77.1%, 80.2%, 80.8% and 81.1%, respectively. The high IRH in specimens with RHA illustrates the strong ability of RHA in moisturizing. This is likely to be attributed partly to the micro-pores of RHA particles, which can adsorb and retain water, and partly to the change of pore microstructure due to the addition of RHA.

Note that IRH is an important parameter in concrete not only for the hydration but also for the durability. The relationships between IRH and concrete properties have been studied by a number of researchers, for instance, [54-56]. Fig.13 shows the correlation of the creep coefficient and IRH obtained from the specimens with

different RHA-to-binder ratios. It can be seen from the figure that, if the region with very high IRH value is excluded, then a linear relationship between these two parameters could be obtained.

### 3.3 Pore microstructure

It is known that the cement paste formed by hydration reactions contains interconnected pores of different sizes, namely the gel pores (a few fractions of a nm to several nm) within C-S-H, capillary pores (tens of nm to several μm), and air voids (greater than tens of μm). The SEM images taken from samples in the specimens with different RHA-to-binder ratios at 180 day curing are shown in Fig.14. It can be observed from these images that, in the sample with no RHA large capillary pores exist. In contrast, in the samples with RHA the sizes of capillary pores are relatively small and they are surrounded and/or filled by C-S-H gel pores produced by cement hydration and secondary pozzolanic reaction of RHA. The higher the RHA added in the binder, the smaller the sizes of capillary pores. This indicates that the addition of RHA in concrete could decrease the porosity of the capillary pores of concrete and thus improve the mechanical and durability properties of the material. This may also explain why the specimens with higher RHA have lower creep and higher IRH, as demonstrated in Figs.7 and 12.

Many RHA particles are much smaller than cement particles as it is demonstrated in

Fig.1. When they are mixed with cement, these small particles can fill the capillary pores of cement paste. In addition, RHA particles are also highly reactive. They react with calcium hydroxide originated from cement hydration to produce additional C-S-H. This additional C-S-H can also fill large pores and/or voids. Furthermore, the release of absorbed water which is retained in the small pores of RHA particles at early days can improve cement hydration and thus reduces the size of interfacial transition zones and the porosity related to gel pores. Fig. 15 shows the effect of RHA on the pore-size distribution, measured by MIP. Note that MIP is a useful tool and can serve as comparative indices for the connectivity and capacity of the pore systems in hydrated cements although it is not accurate in terms of the measures of the actual pore sizes present [57]. Nevertheless, it can be seen from Fig.15 that, the increase of RHA in the mixture leads to a decrease in pore size and/or in pore volume. Table 4 provides a detailed comparison of porosities of different size groups. It is evident that the addition of RHA in concrete can effectively reduce the porosity of large pores.

## 4. Conclusions

This paper has reported the experimental data of the mechanical properties and creep strain of concrete with RHA as a SCM. In addition, the pore microstructure has been analyzed to examine the effect of RHA on the pore size distribution and pore volume of the hardened concrete. From the present study the following conclusions can be drawn:

- Similar to what was reported in literature, the addition of RHA in concrete can improve the compressive strength and modulus of elasticity of the concrete. However, there seems to be an upper limit, above which a further increase of RHA may not lead to further improvement of mechanical properties.
- The creep strain decreases with the increase of RHA added in concrete. However, similar to the increase of modulus of elasticity, the decrease of creep strain with increased RHA is only up to a certain level of RHA.
- The IRH decreases very quickly in the first 60 days, and after then the decrease becomes very slow. The addition of RHA in concrete can reduce the decrease of IRH. There are good correlations between the IRH and creep strain, and the IRH and drying shrinkage strain.
- Due to its small particle sizes and high silicon content, RHA can react with cement hydration products to produce C-S-H, which can fill capillary pores and/or voids in concrete.
- Due to its porous nature, RHA can absorb, retain and release water during the cement hydration process, which can improve the hydration of cement paste and reduce the size of interfacial transition zones in concrete.

**Acknowledgments** - The authors would like to acknowledge the National Natural Science Foundation of China (Grant No. 41427802 and 51602198) and the Shaoxing University Scientific Research Project (Grant No. 20145030) for their financial support to the work present in this paper.

References

[1] N. Soltani, A. Bahrami, M.I. Pech-Canul, L.A. González. Review on the physicochemical treatments of rice husk for production of advanced materials. Chemical Engineering Journal 264 (2015) 899–935.

[2] Y. Shen, P. Zhao, Q. Shao. Porous silica and carbon derived materials from rice husk pyrolysis char. Microporous and Mesoporous Materials 188 (2014) 46–76.

[3] T. Witoon, Polyethyleneimine-loaded bimodal porous silica as low-cost and high-capacity sorbent for CO2 capture. Mater. Chem. Phys. 137 (2012) (1) 235-245.

[4] W. Zeng, H. Bai. Swelling-agent-free synthesis of rice husk derived silica materials with large mesopores for efficient CO2 capture. Chemical Engineering Journal 251 (2014) 1-9.

[5] M. Azadi, M.E. Bahrololoom, F. Heidari. Enhancing the mechanical properties of an epoxy coating with rice husk ash, a green product. J. Coat. Technol. Res. 8 (2011) (1) 117–123.

[6] N. Tipsotnaiyana, L. Jarupan, C. Pechyen. Synthesized silica powder from rice husk for printing raw materials application. Adv. Mater. Res. 506 (2012) 218-221.

[7] F. Bondioli, F. Andreola, L. Barbieri, T. Manfredini, A.M. Ferrari. Effect of rice husk ash (RHA) in the synthesis of (Pr, Zr) SiO4 ceramic pigment. J. Eur. Ceram. Soc. 27 (2007) (12) 3483–3488.

[8] F. Andreola, L. Barbieri, F. Bondioli. Agricultural waste in the synthesis of coral

ceramic pigment. Dyes Pigm. 94 (2012) (2) 207–211.

[9] M. Gonçalves, C. Bergmann. Thermal insulators made with rice husk ashes: production and correlation between properties and microstructure. Constr. Build. Mater. 21 (2007) (12) 2059–2065.

[10] B.I. Ugheoke, E.O. Onche, O.N. Namessan, G.A. Asikpo. Property optimization of kaolin-rice husk insulating fire-bricks. Leonardo Electron. J. Pract. Technol. 5 (2006) 167–178.

[11] H. Haxo Jr, P. Mehta. Ground rice-hull ash as a filler for rubber. Rubber Chem. Technol. 48 (1975) (2) 271–288.

[12] P. Sae-Oui, C. Rakdee, P. Thanmathorn. Use of rice husk ash as filler in natural rubber vulcanizates: in comparison with other commercial fillers. J. Appl. Polym. Sci. 83 (2002) (11) 2485–2493.

[13] F. Adam, J. Andas, I. Rahman. The synthesis and characterization of cobalt-rice husk silica nanoparticles. Open Colloid Sci. J. 4 (2011) 12–18.

[14] S. Bose, H. Acharya, H. Banerjee. Electrocal, thermal, thermoelectric and related properties of magnesium silicide semiconductor prepared from rice husk, J. Mater. Sci. 28 (1993) 5461–5468.

[15] I. Valchev, V. Lasheva, T. Tzolov, N. Josifov. Silica products from rice hulls. J. Univ. Chem. Technol. Metall. 44 (2009) (3) 257–261.

[16] E. Mizuki, S. Okumura, H. Saito, S. Murao. Formation of silicon carbide from rice husks using enzymatic methods for carbon control. Bioresour. Technol. 44 (1993) (1) 47–51.

[17] Y. Liu, Y. Guo, W. Gao, Z. Wang, Y. Ma, Z. Wang. Simultaneous preparation of silica and activated carbon from rice husk ash. J. Cleaner Prod. 32 (2012) 204–209.

[18] S. Das, T. Dan, S. Prasad, P. Rohatgi. Aluminium alloy-rice husk ash particle composites. J. Mater. Sci. Lett. 5 (1986) (5) 562–564.

[19] D. Zhu, M. Gao, S. Zhang, H. Wu, Y. Pan, Y. Liu, H. Pan, F.J. Oliveira, J.M. Vieira. A high-strength SiCw/SiC–Si composite derived from pyrolyzed rice husks by liquid silicon infiltration. J. Mater. Sci. 47 (2012) (12) 4921–4927.

[20] D.G. Nair, A. Fraaij, A.A.K. Klaassen, A.P.M. Kentgens. A structural investigation relating to the pozzolanic activity of rice husk ashes. Cem. Concr. Res. 38 (2008) (6) 861–869.

[21] V. Papadakis, S. Tsimas. Supplementary cementing materials in concrete: Part I: efficiency and design. Cem. Concr. Res. 32 (2002) (10) 1525–1532.

[22] S. Chandrasekhar, P. Pramada, J. Majeed. Effect of calcination temperature and heating rate on the optical properties and reactivity of rice husk ash. J. Mater. Sci. 41 (2006) (23) 7926–7933.

[23] V. Saraswathy, H.W. Song. Corrosion performance of rice husk ash blended concrete. Constr. Build. Mater. 21 (2007) (8) 1779–1784.

[24] M.F.M. Zain, M.N. Islam, F. Mahmud, M. Jamil. Production of rice husk ash for use in concrete as a supplementary cementitious material. Construction and Building Materials 25 (2011) (2)798-805.

[25] R. Zerbino, G. Giaccio, G.C. Isaia. Concrete incorporating rice-husk ash without processing. Construction and Building Materials 25 (2011) (1)371-378.

[26] I.H. Ling, D.C.L. Teo. Properties of EPS RHA lightweight concrete bricks under different curing conditions. Construction and Building Materials 25 (2011) (8)3648-3655.

[27] B. H. Abu Bakar, P. J. Ramadhansyah, M. J. Megat Azmi. Effect of rice husk ash fineness on the chemical and physical properties of concrete. Magazine of Concrete Research 63 (2011) (5)313-320.

[28] H.K. Venkatanarayanan, P.R. Rangaraju. Effect of grinding of low-carbon rice husk ash on the microstructure and performance properties of blended cement concrete. Cement and Concrete Composites 55 (2015) 348-363.

[29] D.D. Bui, J. Hu, P. Stroeven. Particle size effect on the strength of rice husk ash blended gap-graded Portland cement concrete. Cement and Concrete Composites 27 (2005) (3) 357-366.

[30] G.C Isaia, A.L.G Gastaldini, R Moraes. Physical and pozzolanic action of mineral additions on the mechanical strength of high-performance concrete. Cement and Concrete Composites 25 (2013) (1) 69-76.

[31] J.S. Coutinho. The combined benefits of CPF and RHA in improving the durability of concrete structures. Cement and Concrete Composites 25 (2003) (1) 51-59.

[32] G.R. de Sensale. Effect of rice-husk ash on durability of cementitious materials. Cement and Concrete Composites 32 (2010) (9) 718-725.

[33] W. Chalee, T. Sasakul, P. Suwanmaneechot, C. Jaturapitakkul. Utilization of rice husk-bark ash to improve the corrosion resistance of concrete under 5-year exposure in a marine environment. Cement and Concrete Composites 37 (2013) 47-53.

[34] E.R. Grist, K.A. Paine, A. Heath, J. Norman, H. Pinder. Structural and durability properties of hydraulic lime–pozzolan concretes. Cement and Concrete Composites 62 (2015) 212-223.

[35] R.P. Jaya, B.H.A. Bakar, M.A.M. Johari, M.H.W. Ibrahim, M.R. Hainin, D.S. Jayanti. Strength and microstructure analysis of concrete containing rice husk ash under seawater attack by wetting and drying cycles. Advances in Cement Research 26 (2014) (3)145-154.

[36] K.M.A. Hossain, M.S. Anwar. Performance of rice husk ash blended cement concretes subjected to sulphate environment. Magazine of Concrete Research 66 (2014) (24) 1237-1249.

[37] M.E. Rahman, A.S. Muntohar, V. Pakrashi, B.H. Nagaratnam, D. Sujan. Self-compacting concrete from uncontrolled burning of rice husk and blended fine aggregates. Materials & Design 55 (2014) 410-415.

[38] M.F. Nuruddin, K.Y. Chang, N.M. Azmee. Workability and compressive strength of ductile self-compacting concrete (DSCC) with various cement replacement materials. Construction and Building Materials 55 (2014) 153-157.

[39] J. He, Y. Jie, J. Zhang, Y. Yu, G. Zhang. Synthesis and characterization of red mud and rice husk ash-based geopolymer composites. Cement and Concrete Composites 37 (2013) 108-118.

[40] M.A.M. Ariffin, M.A.R. Bhutta, M.W. Hussin, M.M Tahir, N. Aziah. Sulphuric acid resistance of blended ash geopolymer concrete. Construction and Building Materials 43 (2013) 80-86.

[41] A. Nazari, A.F. Rohani. Alkali-activated geopolymer produced by seeded fly ash and rice husk bark ash. Advances in Cement Research 24 (2012) (5)301-309.

[42] G.R. de Sensale, A.B. Ribeiro, A. Gonçalves. Effects of RHA on autogenous shrinkage of Portland cement pastes. Cement and Concrete Composites 30 (2008) (10) 892-897.

[43] Z.P. Bazant. Theory of Creep and Shrinkage in Concrete Structures: A Precise of Recent Developments. Mechanics Today, Vol.2 (Ed by S. Nemat-Nasser), Pergamon Press, Chapter 1, pp1-93, 1975.

[44] S.E. Pihlajavaara. A review of some of the main results of a research on the ageing phenomena of concrete: Effect of moisture conditions on strength, shrinkage and creep of mature concrete. Cement and Concrete Research 4 (1974) (5) 761-771.

[45] J.Y. Li, Y. Yao. A study on creep and drying shrinkage of high performance concrete. Cement and Concrete Research 31 (2001) (8) 1203-1206.

[46] S.B. Santos, L.C.P.S. Filho, J.L. Calmon. Early-age creep of mass concrete: effects of chemical and mineral admixtures. ACI Materials Journal 109 (2012) (5) 537-544.

[47] R.P. Khatri, V. Sirivivatnanon, W. Gross. Effect of different supplementary cementitious materials on mechanical properties of high performance concrete. Cement and Concrete Research 25 (1995) (1) 209-220.

[48] J.J. Brooks, M.A. Megat-Johari. Effect of metakaolin on creep and shrinkage of concrete. Cement & Concrete Composites 23 (2001) (6) 495-502.

[49] M. Shariq, J. Prasad, H. Abbas. Creep and drying shrinkage of concrete containing GGBFS. Cement & Concrete Composites 68 (2016) 35-45.

[50] M.D. Safiuddin, J.S. West, K.A. Soudki. Hardened properties of self-consolidating high performance concrete including rice husk ash. Cement and Concrete Composites 32 (2010) (9)708-717.

[51] D. Chopra, R. Siddique, Kunal. Strength, permeability and microstructure of self-compacting concrete containing rice husk ash. Biosystems Engineering 130 (2015) 72-80.

[52] V. Kannan, K. Ganesan. Chloride and chemical resistance of self compacting concrete containing rice husk ash and metakaolin. Construction and Building Materials 51 (2014) 225-234.

[53] A.L.G. Gastaldini, M.P. da Silva, F.B. Zamberlan, C.Z. Mostardeiro Neto. Total shrinkage, chloride penetration, and compressive strength of concretes that contain clear-colored rice husk ash. Construction and Building Materials 54 (2014): 369-377.

[54] E. Drouet, S. Poyet, J.M. Torrenti. Temperature influence on water transport in hardened cement pastes. Cement and Concrete Research 76 (2015) 37-50.

[55] M. Wyrzkowski, P. Lura. The effect of external load on internal relative humidity in concrete. Cement and Concrete Research 65 (2014) 58-63.

[56] Z.W. Jiang, Z.P. Sun, P.M. Wang. Internal relative humidity distribution in high performance cement paste due to moisture diffusion and self-desiccation. Cement and concrete research 36 (2006) (2)320-325.

[57] S. Diamond. Mercury porosimetry: An inappropriate method for the measurement of pore size distributions in cement-based materials. Cement and Concrete Research 30 (2000) (10) 1517–1525.

Table 1 Chemical compositions of PC and RHA (wt %)

| Materials | $SO_3$ | $SiO_2$ | $Fe_2O_3$ | $Al_2O_3$ | CaO | MgO | $K_2O$ | $Na_2O$ | $TiO_2$ |
|---|---|---|---|---|---|---|---|---|---|
| Cement | 2.54 | 21.10 | 3.26 | 4.77 | 62.63 | 1.15 | 0.43 | 0.05 | 0.28 |
| RHA | 0.19 | 90.20 | 0.82 | 0.38 | 0.91 | 0.32 | 1.59 | 0.19 | 0.07 |

Table 2 Mix proportions of concretes with different RHA (in weight)

| Types of mixture | Cement | RHA | River sand | Crushed granite | Water | Superplasticizer |
|---|---|---|---|---|---|---|
| C | 460 | 0 | 703 | 1053 | 184 | 2.76 |
| C+10RHA | 414 | 46 | 703 | 1053 | 184 | 3.68 |
| C+15RHA | 391 | 69 | 703 | 1053 | 184 | 4.14 |
| C+20RHA | 368 | 92 | 703 | 1053 | 184 | 4.37 |

Table 3 Summary of tests

| Type of tests | Specimen dimensions (mm) | Age of specimens before test (days) | No of specimens tested* |
|---|---|---|---|
| Compressive strength | 150x150x150 | 28 | 3x4 |
| Young’s modulus | 150x150x300 | 28 | 3x4 |
| Creep | 100x100x300 | 7 | 2x2x4 |
| Drying shrinkage | 100x100x300 | 7 | 3x4 |

Note*: 4 is the types of concrete mixtures

Table 4 Distribution of pore size in samples with different RHA (mL/g)

| Number | <100nm | | >100nm | Total porosity |
|---|---|---|---|---|
| | <50nm | (50～100)nm | | |
| C | 0.012 | 0.005 | 0.034 | 0.051 |
| C+10RHA | 0.008 | 0.004 | 0.028 | 0.04 |
| C+15RHA | 0.008 | 0.003 | 0.025 | 0.036 |
| C+20RHA | 0.007 | 0.003 | 0.022 | 0.032 |

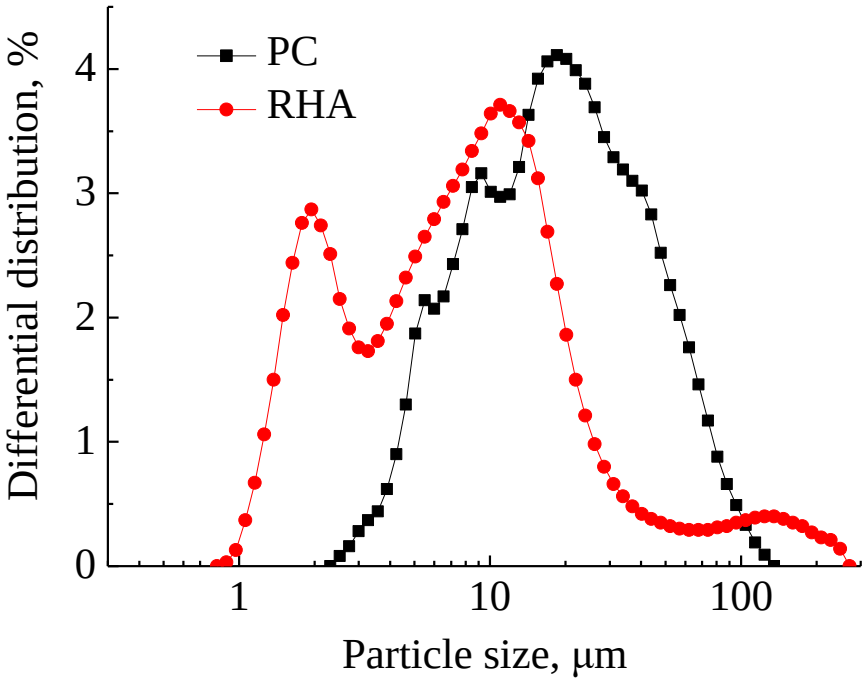


Fig.1 Particle size distributions of PC and RHA.

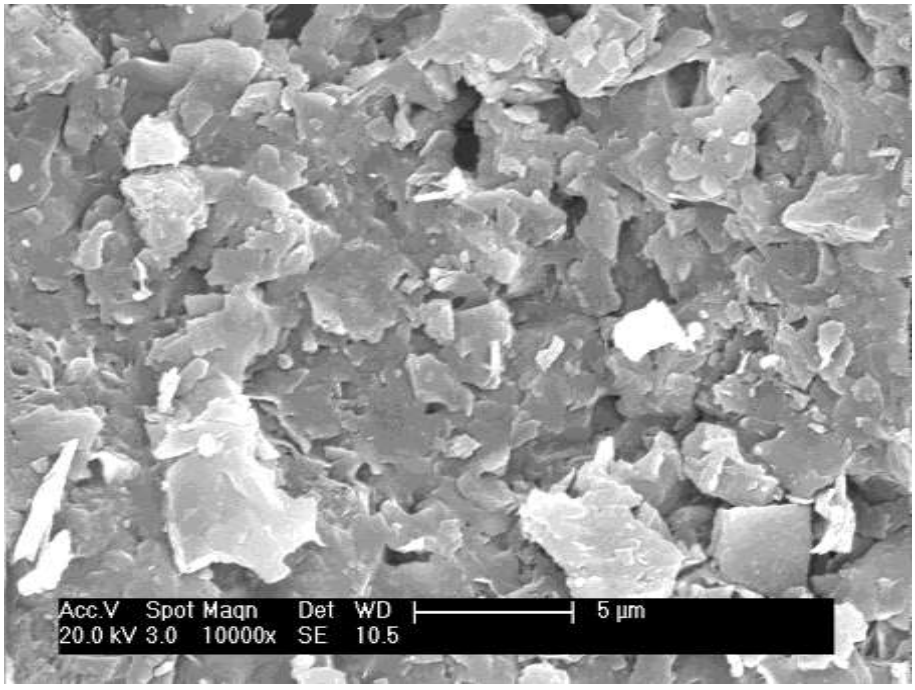

Fig.2 SEM image of RHA.

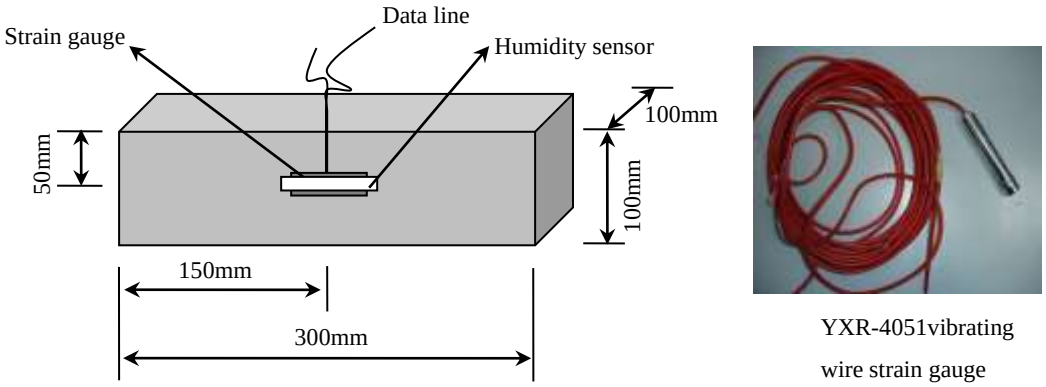


(a)

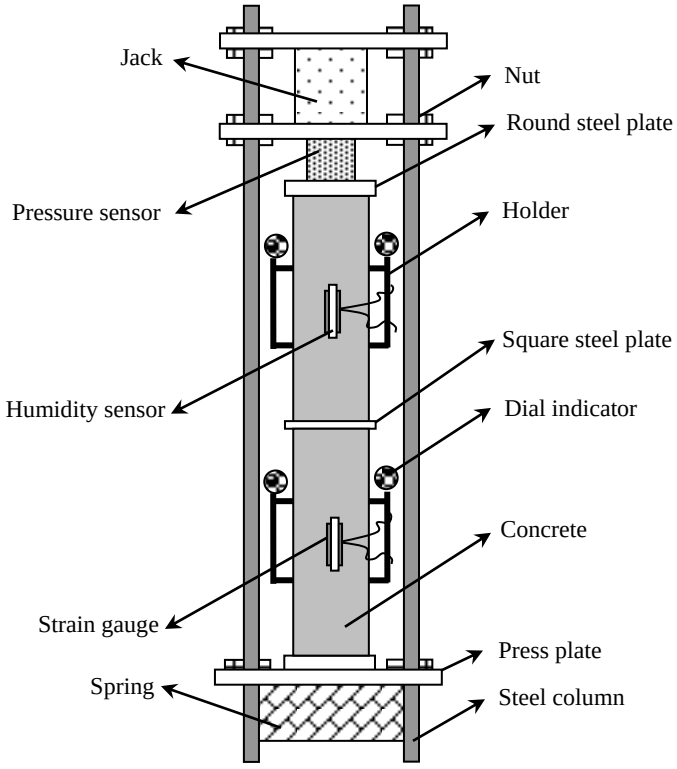


(b)

Fig.3 (a) Specimen prepared for creep test. (b) Experimental setup for creep test.

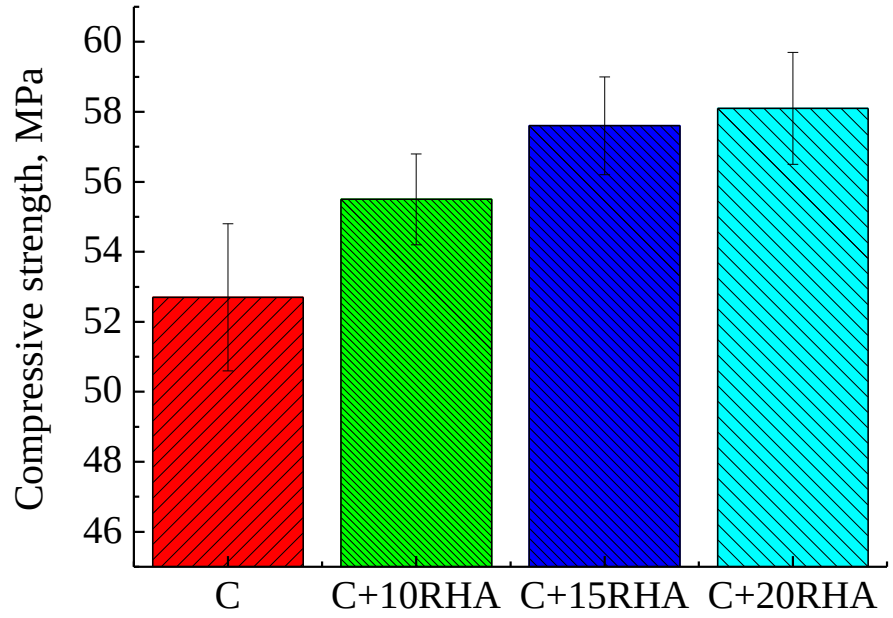


Fig.4 Effect of RHA on compressive strength of specimens at 28 days (error bar represents the variation of test data).

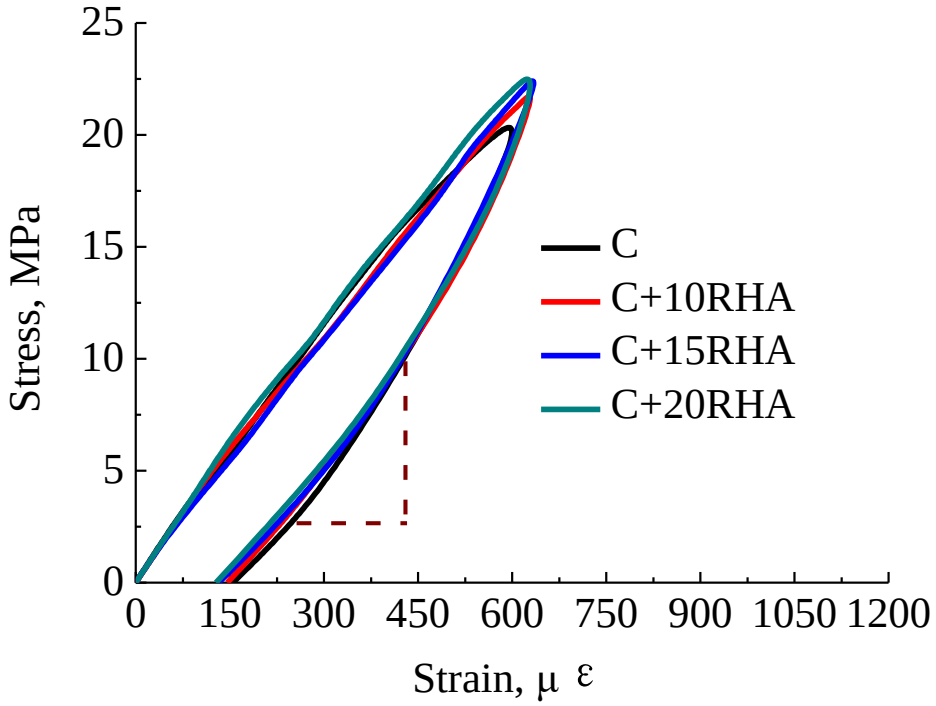


Fig.5 Experimental stress-strain curves for determining Young's modulus.

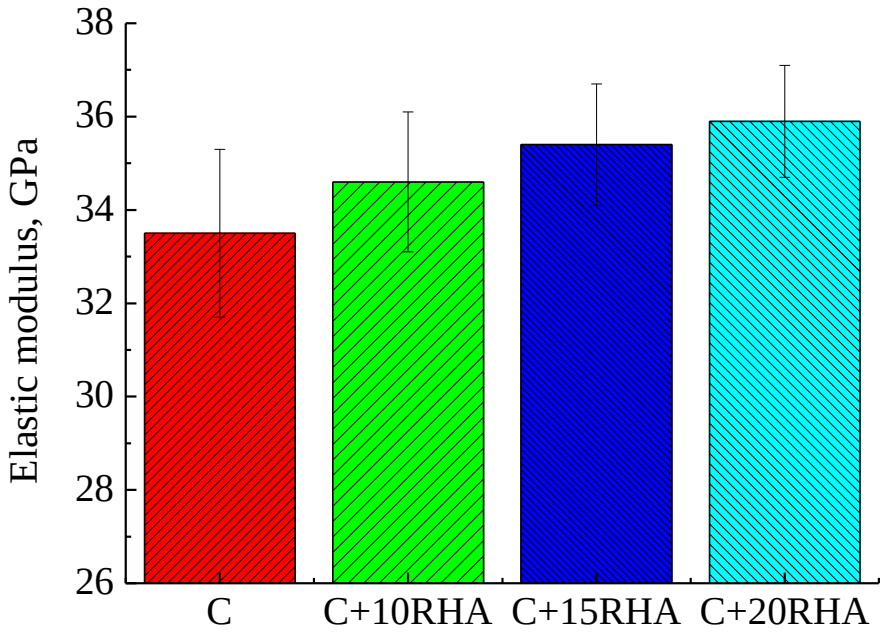


Fig.6 Effect of RHA on elastic modulus of specimens at 28 days (error bar represents the variation of test data).

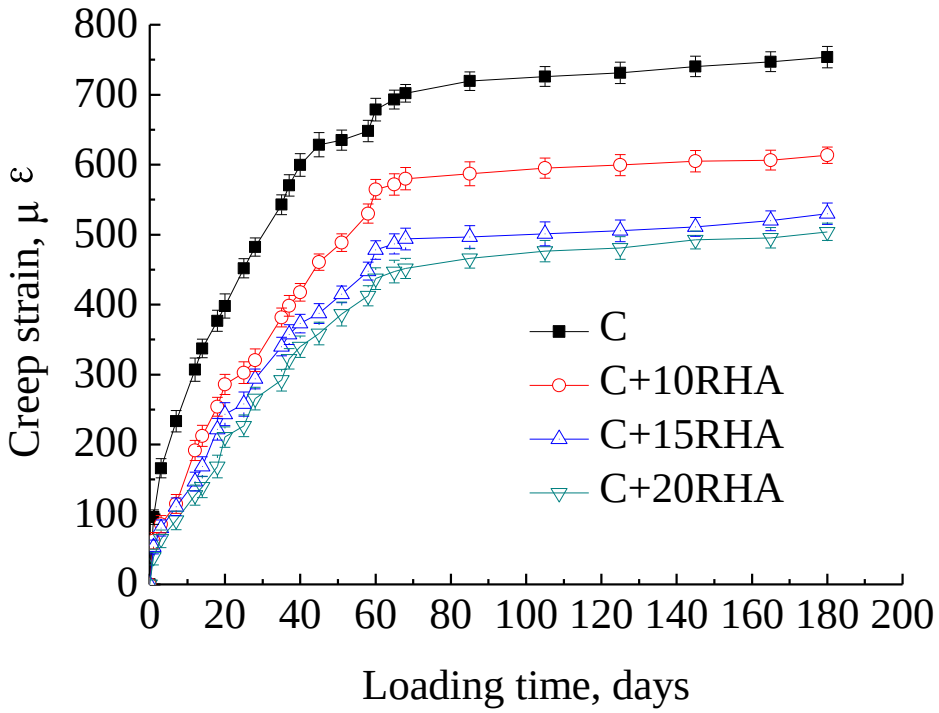


Fig.7 Effect of RHA on creep strain of specimens (error bar represents the variation of test data).

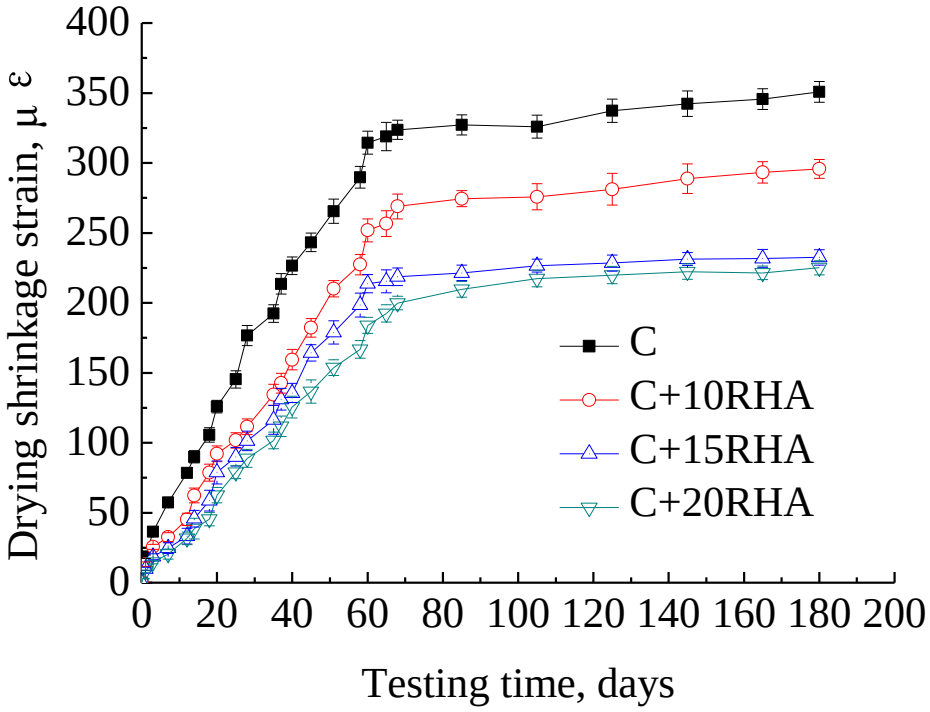


Fig.8 Effect of RHA on drying shrinkage strain of specimens (error bar represents the variation of test data).

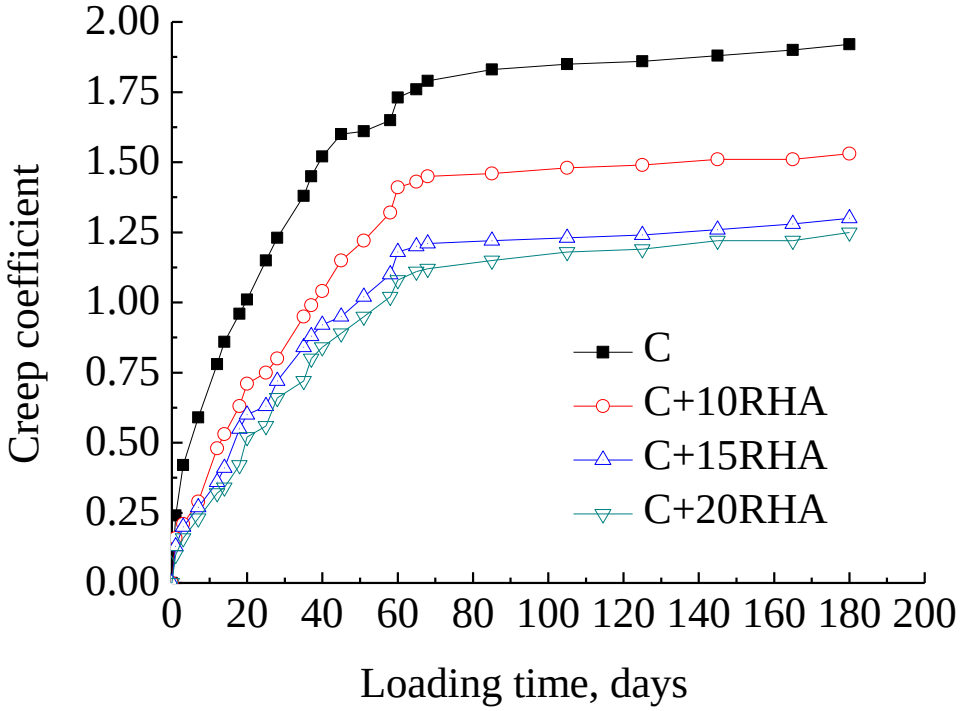


Fig.9 Effect of RHA on creep coefficient of specimens.

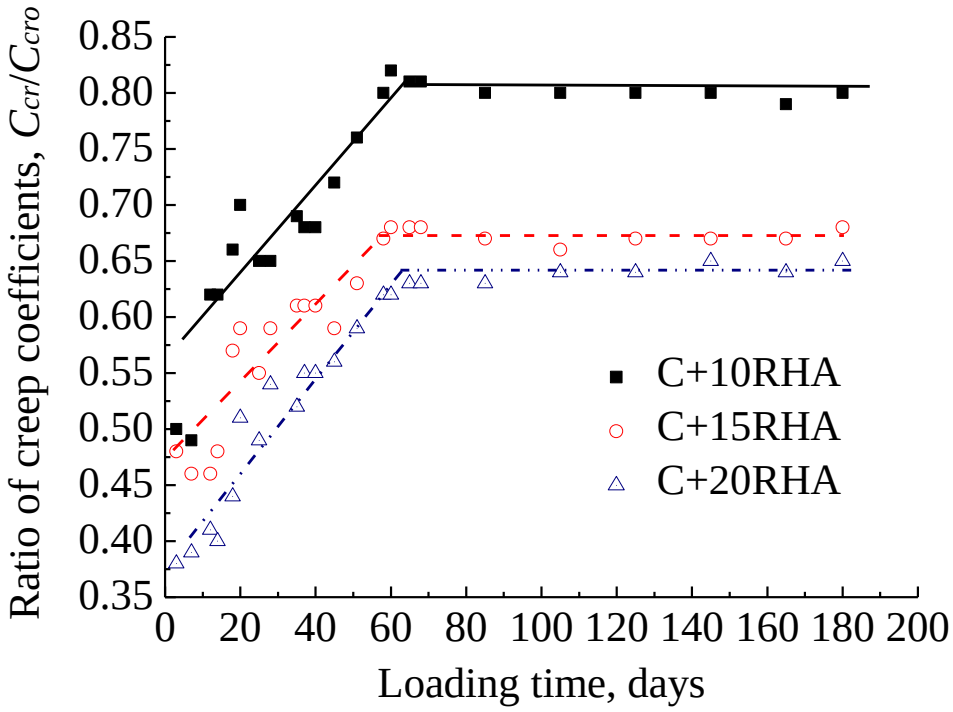


Fig.10 Variation of the ratio of creep coefficients ($C_{cro}$: creep coefficient of specimen without RHA. $C_{cr}$: creep coefficient of specimen with RHA).

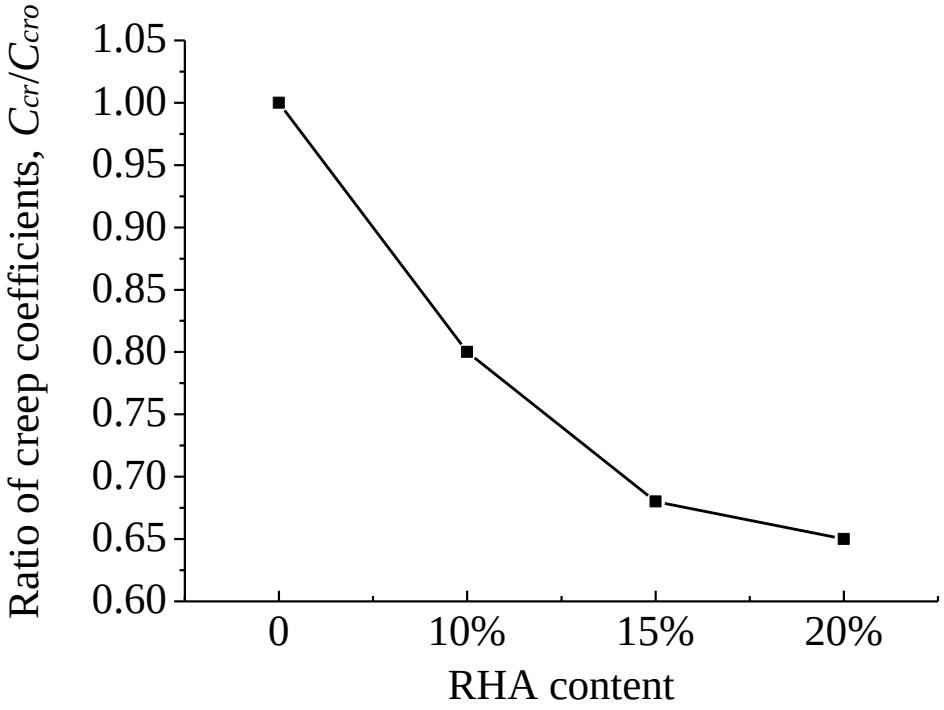


Fig.11 Effect of RHA on the ratio of creep coefficient at 180 days since the loading ($C_{cro}$: creep coefficient of specimen without RHA. $C_{cr}$: creep coefficient of specimen with RHA).

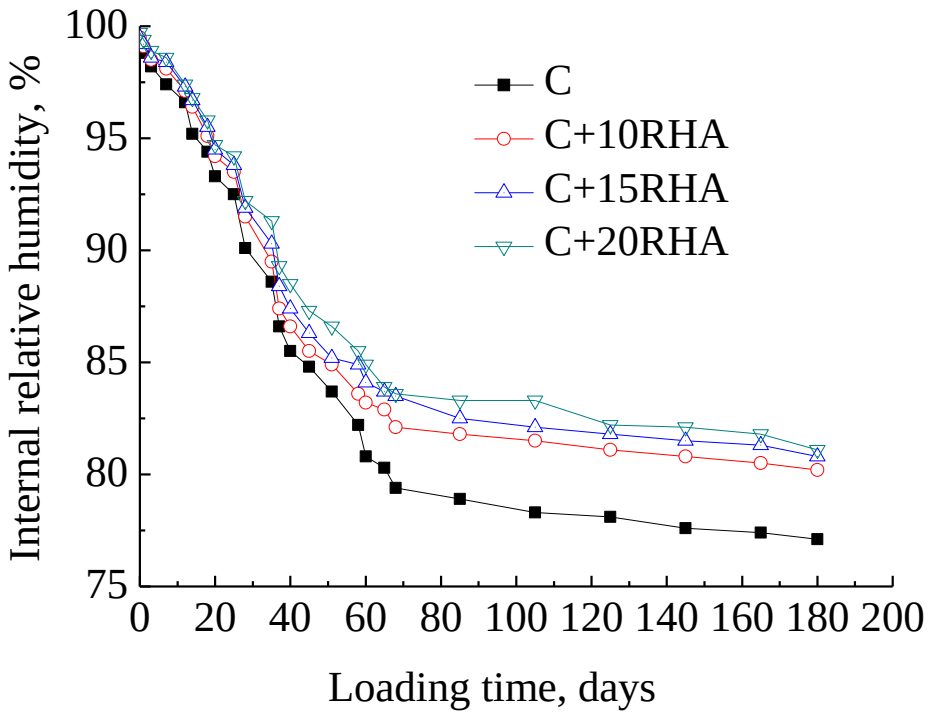


Fig.12 Effect of RHA on IRH of specimens.

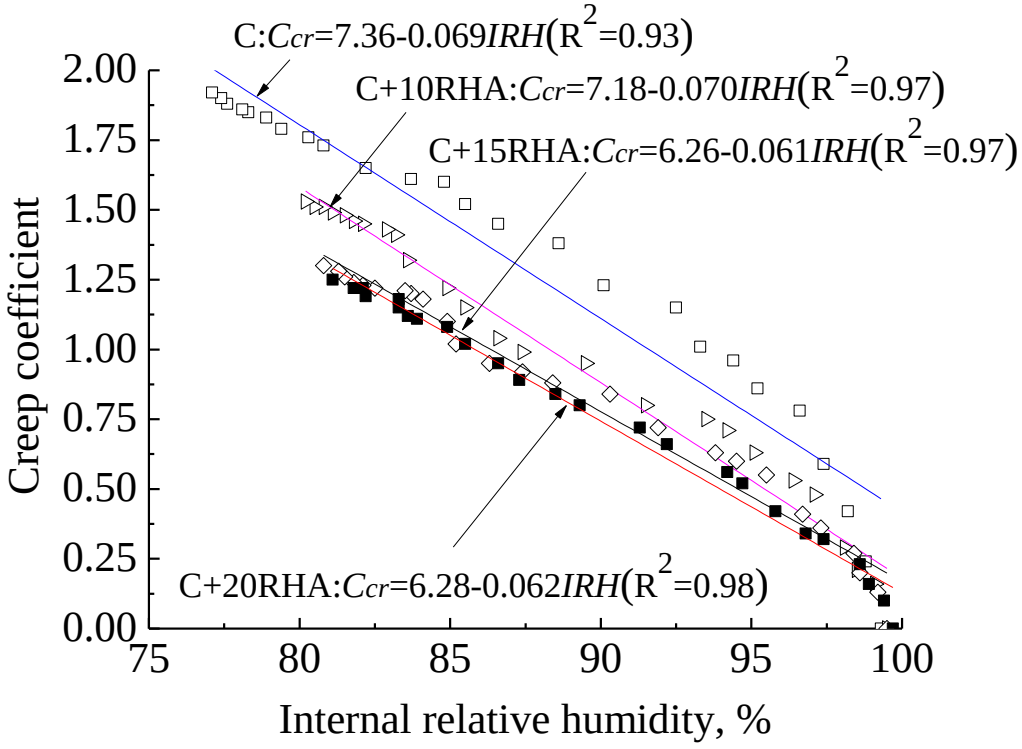


Fig.13 Linear relationship between creep coefficient and IRH.

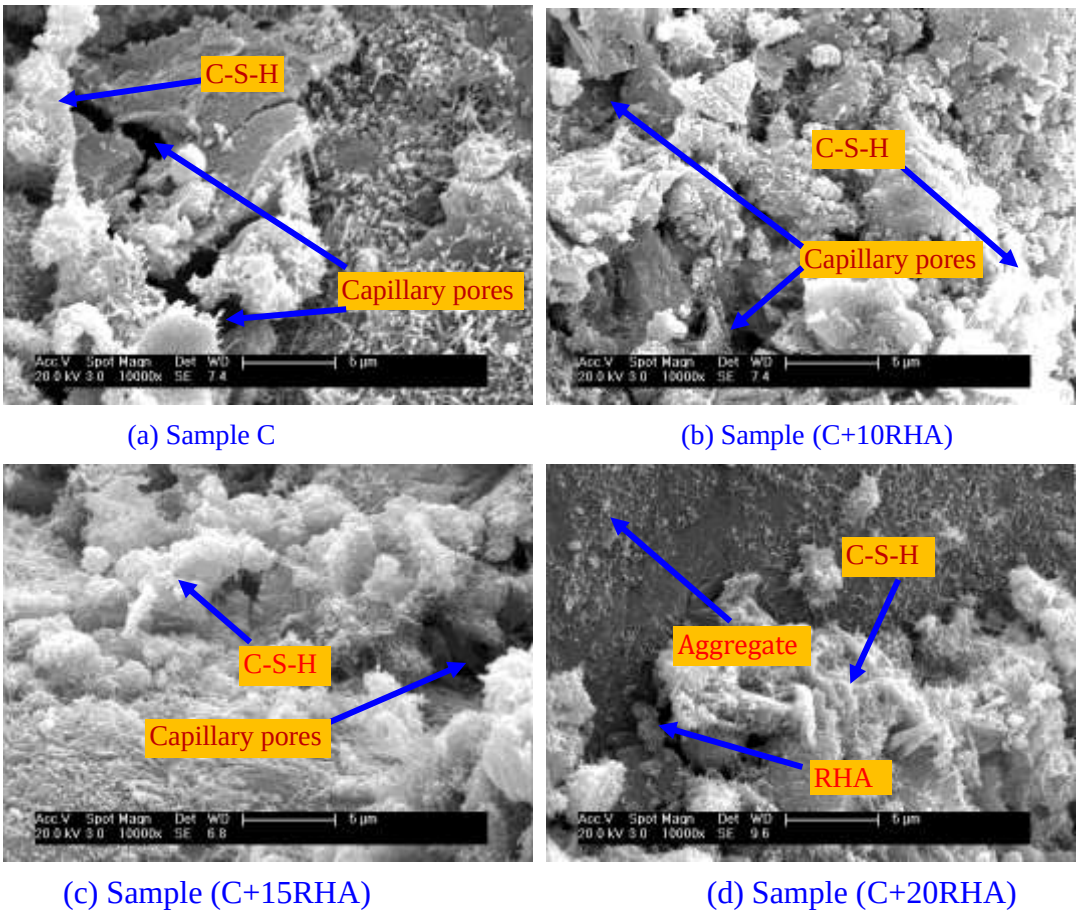


(a) Sample C (b) Sample (C+10RHA)

(c) Sample (C+15RHA) (d) Sample (C+20RHA)

Fig.14 SEM images of specimens of different RHA.

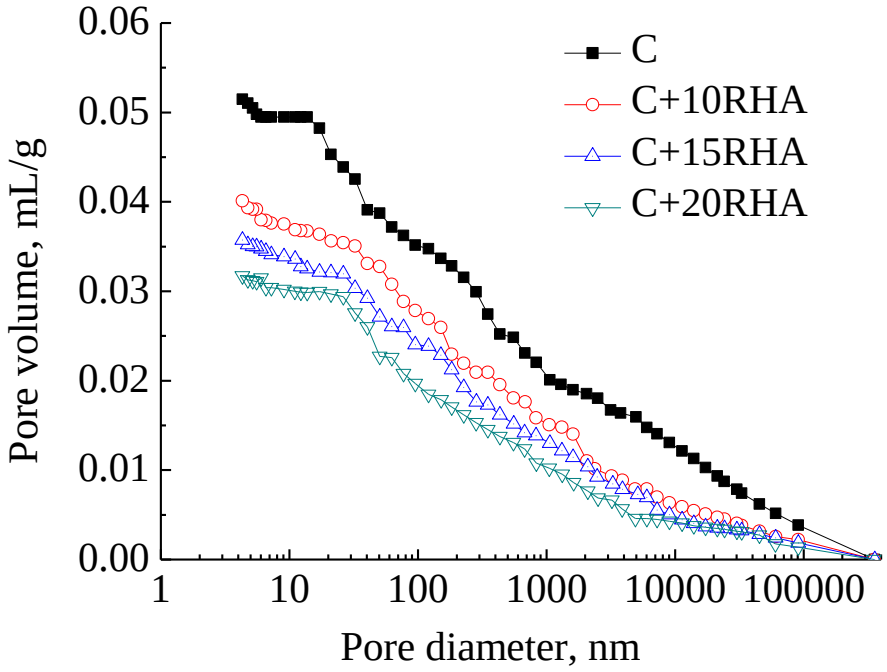


Fig.15 Effect of RHA on cumulative porosity of specimens.